ACS SyntheticBiology

pubs.acs.org/synthbio Research Article

Universal Actuator for Efficient Silencing of *Escherichia coli* Genes Based on Convergent Transcription Resistant to Rho-Dependent Termination

Alexander A. Krylov,* Valeriya V. Shapovalova, Elizaveta A. Miticheva, Mikhail S. Shupletsov, and Sergey V. Mashko

Cite This: *ACS Synth. Biol.* 2020, 9, 1650−1664 Read Online

ACCESS | Metrics & More | Article Recommendations | Supporting Information

ABSTRACT: Dynamic control is a distinguished strategy in modern metabolic engineering, in which inducible convergent transcription is an attractive approach for conditional gene silencing. Instead of a simple strong "reverse" (*r*-) promoter, a three-component actuator has been developed for constitutive genes silencing. These actuators, consisting of *r*-promoters with different strengths, the ribosomal transcription antitermination-inducing sequence *rrnG*-AT, and the RNase III processing site, were inserted into the 3′-UTR of three *E. coli* metabolic genes. Second and third actuator components were important to improve the effectiveness and robustness of the approach. The maximal silencing folds achieved for *gltA*, *pgi*, and *ppc* were approximately 7, 11, and >100, respectively. Data were analyzed using a simple model that considered RNA polymerase (RNAP) head-on collisions as the unique reason for gene silencing and continued transcription after collision with only one of two molecules. It was previously established that forward (*f*-) RNAP with a trailing ribosome was approximately 13-times more likely to continue transcription after head-on collision than untrailed *r*-RNAP which is sensitive to Rho-dependent transcription termination (RhoTT). According to the current results, this bias in complex stabilities decreased to no more than (3.0−5.7)-fold if *r*-RNAP became resistant to RhoTT. Therefore, the developed constitutive actuator could be considered as an improved tool for controlled gene expression mainly due to the transfer of *r*-transcription into a state that is resistant to potential termination and used as the basis for the design of tightly regulated actuators for the achievement of conditional silencing.

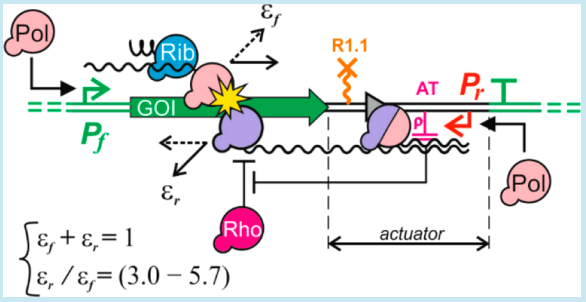

KEYWORDS: *dynamic metabolic control, antisense transcription, gene silencing, antitermination, head-on collisions between RNA polymerases*

The essence of metabolic engineering is the directional redistribution of cellular fluxes into targeted pathways. Today, special attention is paid to controlling this redistribution in response to cellular states, which mimics native regulatory networks. The pioneering work of Farmer and Liao[1] clearly demonstrated the advantages of a strategy that is now called the dynamic control approach.[2] This approach may include not only concertedly induced expression but also conditional silencing of a set of targeted genes of interest (GOIs).[3]

To date, tools for highly efficient conditional gene silencing in *E. coli* have been developed, and they include a large set of *cis*- and *trans*-strategies. The *cis*-strategies include tools for which it is necessary to perform specific editing within the structure of the GOI for targeting; the *trans*-strategies combine genetic elements with structures that do not overlap with the GOI, and only the properly arranged linkage of native and synthetic elements is essential for the final design of the silenced gene.

Members of the *cis*-strategy group are based on degradation tags in the N- or C-terminus or the intraspace[4−6] of the target protein product, riboswitches,[7] native or synthetically regulated promoters in artificial genetic circuits directly governed transcription of GOIs.[8] *Cis*-strategy applications require well-developed and precise tools for host genome editing. However, their prominent advantage is that their efficiency usually does not rely on the plasmid expression systems required for most *trans*-strategies.

Trans-strategies are based on specifically adjusted regulatory proteins (TALE,[9] dCas9[10]), RNAs (*trans*-antisense RNAs (*trans*-asRNAs),[11] and parallel complementary RNAs

Received: November 18, 2019
Published: May 22, 2020

https://dx.doi.org/10.1021/acssynbio.9b00463
ACS Synth. Biol. 2020, 9, 1650−1664

(pRNAs)[12]) or, finally, artificially arranged convergent transcription (CT)-initiated from forward (*f*-) and reverse (*r*-) promoters located in the 5′- and 3′-untranslated regions (UTRs) of the GOI, respectively. Most *trans*-strategies could easily be applied to bacteria with imperfectly developed genome editing tools because their essential components could be and are usually expressed from plasmids. However, the application of these strategies is more suitable for research or small-scale fermentation processes than for large-scale bulk processes. The apparent difference in CT-based strategies compared with other *trans*-strategies is the independence from plasmid usage and, at the same time, a minimal invasion into the native structure of the GOI. Indeed, the *r*-promoter could be integrated outside of a GOI, for example, downstream of the intrinsic transcription terminator (ITT).

There are two general mechanisms of mutual influence for two convergent, overlapping transcriptional units that ultimately result in CT silencing of GOIs: asRNA,[13] which functions both *in cis* and *in trans*, and *cis*-acting transcriptional interference (TI).[14] Moreover, there are examples of CT silencing caused by the two of these mechanisms working concertedly.[15,16]

The former mechanism is based on the ability of the generated asRNA to decrease the expression of a GOI by specifically interacting with mRNA, resulting in a change in its stability or transcription/translation efficiency.[13] Three members of the known set of TI mechanisms[17] are usually described as possible causes of CT-mediated silencing when *f*-/*r*-promoters are separated, with two at the initiation phase of transcription and the third at the elongation stage: (*i*) promoter occlusion, (*ii*) sitting duck interference; or the dislodgement of an initiating RNAP complex, and (*iii*) collisions between converging RNAPs. According to the existing stochastic TI model,[18] occlusion and collisions can produce significant interference if the *r*-promoter is very strong or if converging promoters are far apart (>200 bp), respectively. Taking into account these modeling results, a simplified silencing model, which was used in the present study, considers collisions as the dominant mechanism of TI when promoters are >200 bp apart[15] and neglects other TI mechanisms. A more complicated silencing model particularly considers complex relationships between different TI mechanisms.[19]

Certainly, efficient silencing can be achieved via an RNA−RNA interaction or TI alone; however, both frequently contribute to the total effect although their exact impact ratio is rather difficult to evaluate precisely. Currently, the evaluated impact of RNA interactions from the achieved silencing ranged from zero[18] to no more than half.[15] Collision-based silencing is likely most important when asRNA does not have specific regulatory features, such as interaction loops and hairpins, Hfq binding motifs, or RNase processing sites.[15]

Although GOI silencing mediated by CT was discovered in bacteria many years ago,[20] only a few practical applications have been published in over two decades,[21,22] for example, designing a variant of a tightly regulated expression vector plasmid. In contrast, there are publications investigating CT mechanisms in bacteria,[17,23,24] and their usage for the controlled expression of reporter genes.[15,16,22] The application of this strategy might be broadened in the near future because its power as a modulator for genetic circuits was recently clearly demonstrated.[15] However, one of the important bottlenecks for CT is the possibility of untimely Rho-dependent transcription termination (RhoTT)[19] of RNAP initiated from the *r*-promoter.

To our knowledge, the present study, as a continuation of a previously published one,[25] is the first demonstration of the advantages of applying a CT-based strategy for silencing genes with *r*-transcription protected from RhoTT; this strategy could be interesting from a metabolic engineering perspective.

As the first stage of improving conditional silencing tools, the aim of the present study was to design and demonstrate the usability of the universal device *Actuator* for "constitutive" gene silencing based on CT protected from RhoTT. This study aims to reveal the integration of the designed actuators in the 3′-UTRs of three well-known *E. coli* metabolic genes, *gltA*, *pgi*, and *ppc*, and to investigate the individual and multiple silencing efficiencies caused by CT initiated from *r*-promoters of different strengths. The developed actuators consisted of (*i*) O_{lac}-carrier, but not tightly repressed *r*-promoters with different strengths (used in the current study as constitutive promoters, that is, working at the determined level of isopropyl-*β*-D-thiogalactopyranoside (IPTG), e.g., 0 or 0.5 mM), that significantly exceeded each tested GOI *f*-promoter strength; (*ii*) a ribosomal antitermination-inducing sequence from the *E. coli rrnG* ribosomal operon, *rrnG*-AT;[26] and (*iii*) an RNase III processing site from the T7 phage genome, R1.1,[27] inserted in the 3′-UTR instead of the ITT_{GOI} in the opposite direction of the *r*-promoter. The application of these universal constitutive actuators for GOI repression resulted in silencing folds comparable to those of the best experimental examples obtained by other approaches, which are possibly more sophisticated than those used in this study. Moreover, using the simple model of CT silencing with the main assumptions that (*i*) collisions dominantly influenced silencing efficiency and (*ii*) only one of two RNAPs survived each head-on collision, the obtained experimental results were used for comparative evaluation of RNAP dissociation probabilities in the process of head-on collision. It was previously established[19] that *f*-RNAP with a trailing ribosome was approximately 13 times more likely to continue transcription after a head-on collision than untrailed *r*-RNAP, which is usually sensitive to RhoTT. According to the results obtained in the current study, this bias in complex stabilities decreased to no more than (3.0−5.7)-fold if the still-untrailed *r*-RNAP became resistant to RhoTT. Therefore, the developed actuator could be considered as a significantly more efficient tool for CT silencing than the previously applied strategy, mainly due to the transition of the *r*-transcription into a state that is resistant to RhoTT.

RESULTS AND DISCUSSION

Description of Experimental System Elements. Previously, temperature-inducible silencing of the native expression of the *E. coli pykF* gene, encoding pyruvate kinase I from carbon central metabolism, was convincingly demonstrated by *r*-transcription from λP_L[25] as a strong *r*-promoter. In that example, the unique feature was the transition of *r*-RNAP into an elongation complex that is resistant to RhoTT due to the introduction of *rrnG*-AT[26] at the 5′-end of nascent nontranslated $asRNA_{pykF}$. The significant negative influence of the total silencing of RhoTT has been proposed and recently clearly demonstrated for the CT-based approach.[19] Note that to maintain the intact native expression level of a GOI in noninduced silencing conditions, a previous genetic element was inserted just downstream of the native ITT of the GOI,

https://dx.doi.org/10.1021/acssynbio.9b00463
ACS Synth. Biol. 2020, 9, 1650−1664

Table 1. *E. coli* Strains Used in the Study

genotype[a]	abbreviation in article[b]	ref
MG1655	*gltA*(wt) or *pgi*(wt) or *ppc*(wt) or together	VKPM B6195
For Promoter Strength Estimation:		
MG1655 with *yciI*::P_{pgi}-*zsgreen*	P_{pgi}-zsg	this study
MG1655 with *yciI*::P_{gltA}-*zsgreen*	P_{gltA}-zsg	this study
MG1655 with *yciI*::P_{ppc}-*zsgreen*	P_{ppc}-zsg	this study
MG1655 with *yciI*::P_{tac}-*zsgreen*	P_{tac}-zsg	this study
MG1655 with *yciI*::P_{Ltac}-*zsgreen*	P_{Ltac}-zsg	this study
For Silencing Efficiency Estimation:		
MG1655 with *gltA*>R1.1>*λattB*	*gltA*(R1.1)	this study
MG1655 with *gltA*>R1.1>*λattB*-<*rrnG*-AT-<P_{tac}	*gltA*(R1.1)<P_{tac}	this study
MG1655 with *gltA*>R1.1>*λattB*-<*rrnG*-AT-<P_{Ltac}	*gltA*(R1.1)<P_{Ltac}	this study
MG1655 with *pgi*>R1.1>*λattB*	*pgi*(R1.1)	this study
MG1655 with *pgi*>R1.1>*λattB*-<*rrnG*-AT-<P_{tac}	*pgi*(R1.1)<P_{tac}	this study
MG1655 with *pgi*>R1.1>*λattB*-<*rrnG*-AT-<P_{Ltac}	*pgi*(R1.1)<P_{Ltac}	this study
MG1655 with *ppc*>R1.1>*λattB*	*ppc*(R1.1)	this study
MG1655 with *ppc*>R1.1>*λattB*-<*rrnG*-AT-<P_{tac}	*ppc*(R1.1)<P_{tac}	this study
MG1655 with *ppc*>R1.1>*λattB*-<*rrnG*-AT-<P_{Ltac}	*ppc*(R1.1)<P_{Ltac}	this study
MG1655 with *gltA*>R1.1>*λattB*-<*rrnG*-AT-<P_{Ltac}, *pgi*>R1.1>*λattB*-<*rrnG*-AT-<P_{Ltac} and *ppc*>R1.1>*λattB*-<*rrnG*-AT-<P_{tac}	n.a.	this study
MG1655 with *pgi*>R1.1>*λattB*-<*rrnG*-AT(boxA-6UG)-<P_{Ltac}	*pgi*(R1.1)<(AT^{mut})P_{Ltac}	this study

[a]The names of individual genetic elements are separated by a dash (-). The symbols ">" and "<" indicate the direct and reverse action direction of the preceding and following element, respectively. [b]n.a. – not applied.

and each *r*-RNAP must pass through a reversed ITT (Figure 1A). However, if a GOI has a bidirectional ITT, it reduces the efficiency of silencing by termination of some *r*-RNAP, even resistant to RhoTT, but not to ITT, before it collides with *f*-RNAP. To make the previously constructed genetic element simultaneously increasingly robust and safe for the native expression of the GOI, improved designs for the silencing actuator must include the following parts (in the 5′→3′ order): (i) the chosen *r*-promoter, (ii) *rrnG*-AT, (iii) the *λattB* site retained as a scar after λXis/Int-dependent selective marker excision (Methods), and (iv) the inversely oriented RNase III processing site R1.1, originating from the T7 genome[27] (Figure 1B). It was assumed that cleavage at a primary site within the internal loop of R1.1 forms a short hairpin at the 3′-end of nascent mRNA, which protects it from 3′-5′ exonucleolytic degradation, similar to T7 gene *1 in vivo*.[28] This genetic element mitigates the absence of the ITT_{GOI}.

As a result of the application of novel actuators, initiated *r*-RNAP and *f*-RNAP for any GOI passed through complementary and direct R1.1 sequences, respectively. Additionally, the absence of ITT inside the selected R1.1 sequence in both the forward and reverse directions was confirmed by ARNold computer software.[29]

The well-known O_{lac}-carrier P_{tac} and hybrid P_{Ltac} promoters, as a part of designed actuators, were integrated into the chromosome of *E. coli* MG1655 ($lacI^{wt}$) and used in the current study (Figure 1C) to test silencing efficiency for the wide range of *r*-promoter strengths due to cultivation of bacteria in medium with/without IPTG addition. The P_{Ltac} promoter is a stronger version of P_{tac} that was constructed earlier in our laboratory by the fusion of P_{tac} with the upstream part of λP_L (Methods). Note that the 5′-end of nascent *r*-RNA originating from both promoters is the same. The partial repression by the LacI repressor and the possibility of increasing both promoter strengths by IPTG addition (indicated by (+) after the corresponding promoter name below) mimics the application of four constitutive *r*-promoters with different strengths, because of the presence of the chromosomally encoded *lacI* gene of the wild-type.

To test the universality and robustness of the designed actuator for silencing, three *E. coli* genes from central carbon metabolism, *gltA*, *pgi*, and *ppc*, were chosen as the targets. *GltA*, *pgi*, and *ppc* encode citrate synthase, glucose-6-phosphate isomerase, and phosphoenolpyruvate carboxylase, respectively, which use 5 of 13 well-known main biosynthetic metabolite-precursors as substrates during bacterial growth on glucose. Undoubtedly, changing the enzymatic activity of the mentioned gene products by gene silencing could significantly modify biomass accumulation and metabolism, which is why these genes are repeatedly considered models for conditional silencing via different strategies.[30]

The transcriptional strength of the λP_L, P_{tac}, and P_{Ltac} promoters and native promoters of the genes *gltA*, *pgi*, and *ppc* were determined experimentally in appropriate isogenic strains (Table 1, Methods). Candidate *r*-promoters with/without IPTG addition were significantly stronger than the *f*-promoters and exhibited approximately 75%, 50%, 25%, and 5% of the λP_L promoter strength (Figure 2).

Our growth conditions resulted in approximately 1.0 doublings/h growth. Thus, the absolute transcriptional strength of λP_L in such conditions could be estimated as 0.5 transcripts initiated per second (transcr/s) on the basis of previously published data[31−33] (Methods). Finally, the absolute transcriptional strength of the *r*-promoters used was obtained by a simple proportion without consideration of transcriptional bursting.[34] It was found that initiation from the *f*-promoter used in the present study is usually rarer than initiation from the *r*-promoter (Figure 2). The weakest *r*-promoter, $P_{tac}(-)$, initiates transcription no more often than once every 45 s, and the strongest *f*-promoter, P_{ppc}, initiates transcription no more than once every 2.4 min.

A set of isogenic *E. coli* strains was constructed in the present study from the MG1655 wild-type strain and named according to the following formula: GOI(state of its 3′-UTR)<*r*-promoter type (Table 1, Methods).

In the case of the *gltA* and *ppc* genes, the predicted ITTs[35] were saved and moved downstream relative to the GOI direction by actuator insertion. Such a design might be recommended as optimal for future applications. In the case of the *pgi* gene, the predicted ITT and repetitive extragenic palindrome (REP) were completely removed simultaneously with actuator insertion.

The first group of newly constructed mutant strains did not contain *r*-promoters but had an R1.1 site at the 3′-UTR of the GOIs and was constructed to investigate how the presence of R1.1 mitigated the absence of ITT_{GOI} (Figure 3A). The second group, which carried the R1.1 site and inactive actuators due to the presence of an excisable Cm^R marker (with the Shine

https://dx.doi.org/10.1021/acssynbio.9b00463
ACS Synth. Biol. 2020, 9, 1650−1664

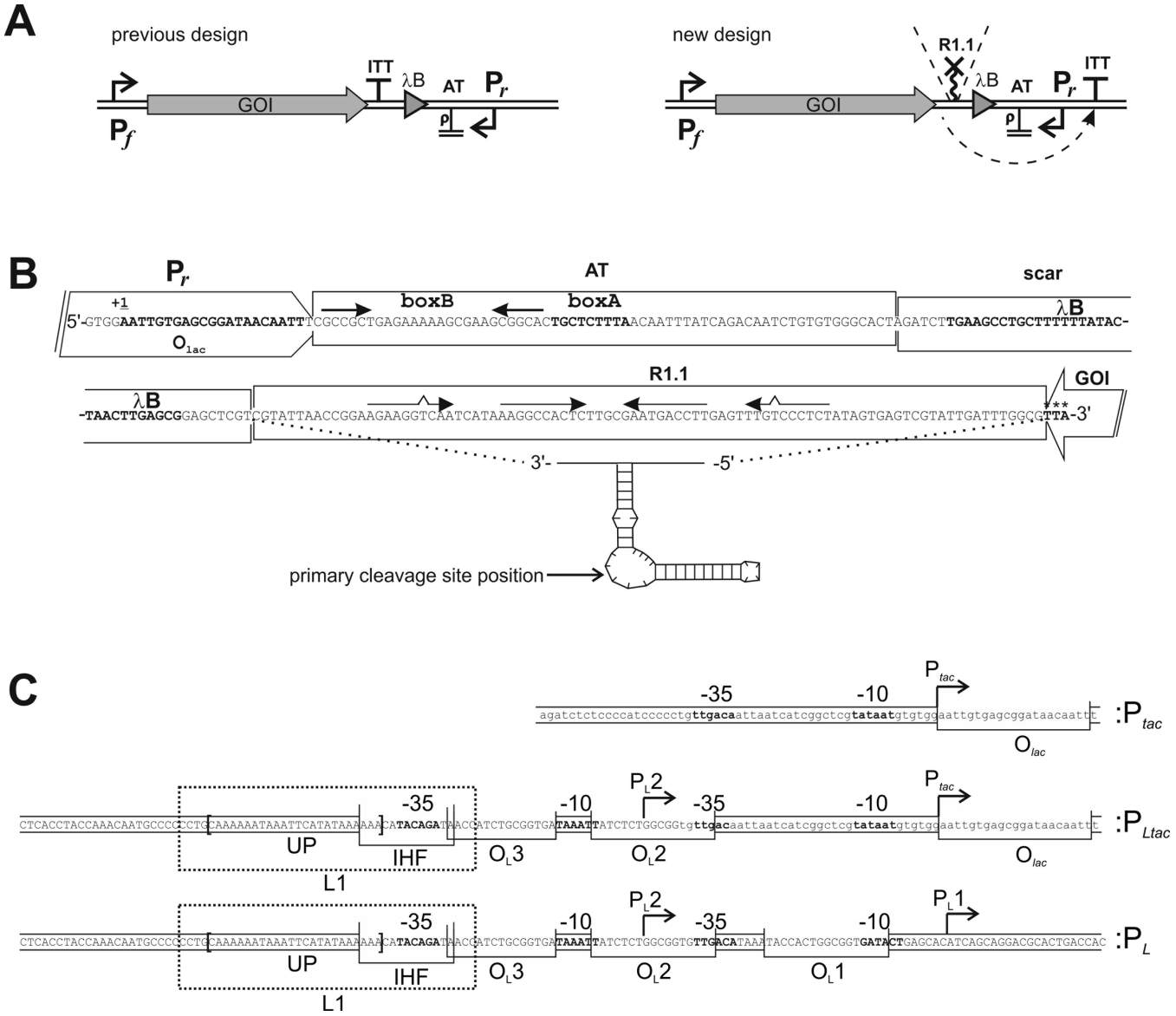

Figure 1. Description of the actuator elements. (A) Elements of the previously used actuator (left) and the actuator from the current study (right). Insertion of the RNase III processing site with a simultaneous moving native internal transcription terminator is shown by dashed arrows. (B) Elements of the actuator and its position relative to any GOIs in the current study: *r*-promoter (P_r); the ribosomal antitermination-inducing sequence *rrnG*-AT with highlighted boxA (bold) and boxB (solid horizontal arrows above) sites; "scar" indicates the sequence resulting after λXis/Int-mediated marker excision with the highlighted recombination site *λattB* (λB); complementary sequence of R1.1, the RNase III-mediated processing site (R1.1). The positions of RNA hairpins formed directly on the R1.1 sequence and the position of the corresponding primary processing site are depicted by solid horizontal and vertical arrows, respectively. Folding of the 3′-UTR $mRNA_{GOI}$ secondary structure leading to formation of RNase III processing site is schematically presented in the bottom part, as well. (C) Sequences of P_{tac}, P_{Ltac}, and P_L promoters used in the study. Operators for binding LacI (O_{lac}), CI/Cro (O_L1, O_L2, O_L3), the recognition site of IHF, and the UP element are depicted.

Dalgarno (SD)-sequence and structural part of the *cat* gene from Tn9 bracketed by *λattL*/*attR* and consisting of a strong $P_{T7,A2}$ promoter and high-efficient ITT_{thrL} at the 5′- and 3′-regions of the gene,[36] respectively), that was used for selection of the target construct (Figure 3B). The third group of strains was obtained after λXis/Int-dependent curing of the marker from the group II strains and contained the fully functional actuator(s) for testing the effect of CT-based silencing on mutant strains (Figure 3C).

Individual and Simultaneous Silencing of *gltA*, *pgi*, and *ppc* genes. Silencing experiments with constructed mutant strains were conducted as follows. Briefly, overnight cultures without IPTG were split into the same fresh medium supplemented or not with 0.5 mM IPTG with a starting OD_{600} of 0.025 and were allowed to continue growing at 37 °C. It was experimentally determined that the novel enzyme concentration was stabilized at 6.0, 5.0, and 5.5 h for *gltA*, *pgi*, and *ppc*, respectively, after it seeded in IPTG-supplemented medium (Methods). Numerically, the efficiency of CT-mediated gene silencing could be evaluated through the experimentally measured parameter designated silencing fold, θ_M:

$$\theta_M = {[EnzAct]_0}/{[EnzAct]_1}$$

where the numerator and denominator of this fraction are the measured enzyme activity of the corresponding wild-type (0)

https://dx.doi.org/10.1021/acssynbio.9b00463
ACS Synth. Biol. 2020, 9, 1650−1664

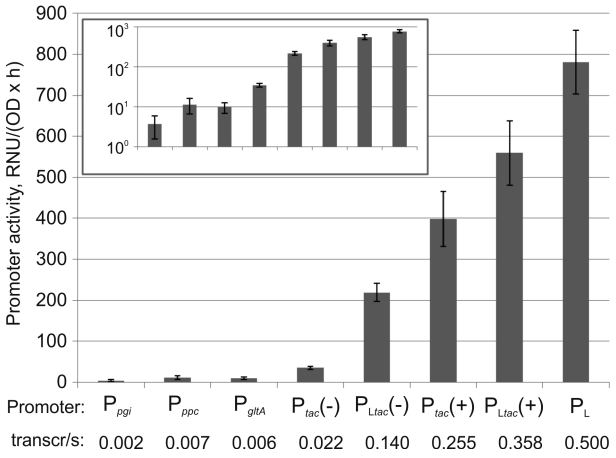

Figure 2. Relative transcriptional strength of the promoters used in this study. For promoters P_{tac} and P_{Ltac}, the absence and presence of 0.5 mM IPTG in the cultivation medium are indicated by (−) and (+) after the corresponding names, respectively. The number at the bottom represents the calculated promoter strength (ϕ), [transcr/s].

and actuator-modified (1) GOI, respectively, under the same conditions.

According to the obtained results, the insertion of the R1.1 RNase III processing site practically did not change the native expression level for all three GOIs under all conditions (Figure 4). Therefore, it was proposed that the substitution of the R1.1 site for the native ITT was mostly safe for many GOIs, and thus, R1.1 was fixed in the minimal composition of the novel actuator. From an engineering perspective, it was rather important because of the standardized position of insertion of the whole actuator, excluding potential termination of transcription initiated from the *r*-promoter due to elimination of the native 3′-UTR_{GOI} and thus making the general silencing efficiency independent of the exact 3′-UTR_{GOI} structure.

As expected, for each GOI, the increase in silencing fold was mainly directly proportional to the estimated *r*-promoter strength (Figure 4).

Additionally, nonlinearly increasing θ_M with increasing length of GOI was observed. Comparison of the silencing fold for the actuator with the weakest *r*-promoter, $P_{tac}(-)$, $[\theta_M]^{gltA}_{P_{tac}(-)}/[\theta_M]^{pgi}_{P_{tac}(-)}/[\theta_M]^{ppc}_{P_{tac}(-)}$ = 1.0:1.3:3.8 to their relative lengths of 1:1.1:1.6 (Supporting Information, Table S1) matched well with the expectation of exponential dependency published previously according to mathematical models proposed on the basis of analogous investigations.[15,18] Nevertheless, the presented statistics were very poor for quantitative representation of the dependency law for TI with extracted impact from mRNA−asRNA interaction.

Interestingly, the application of the three strongest *r*-promoters to the *ppc* gene resulted in an almost undetectable level ($\theta_M \geq 100$) of the retained activity for the corresponding enzyme. However, for these three promoters, a dependence between the increase in *r*-promoter strength and decrease in cellular growth rates was clearly observed. Indeed, aliquots of cultures of *ppc*-silenced strains, for which the activity of the corresponding enzyme was measured in parallel, were seeded again into the same fresh medium, and growth curves were recorded (Methods, Supporting Information, Figure S1A). Note that progenitor strains carrying the inactive Cm^R-carrier forms of different actuators at the end of the *ppc* gene grew identically (Figure S1B). A corresponding relationship between *r*-promoter strength and growth rate for strains with the other two tested genes (*gltA* and *pgi*) was detected only when the retained activity of corresponding enzymes was lower than 20% of the measured activity in wild-type cells (Figure S1C,D).

This phenomenon correlated well with the data confirming that many metabolically regulated enzymes operate below their maximal catalytic potential and that cells maintain costly reserve flux capacities in "turned-off" enzyme molecules to respond rapidly.[37]

Generally, the obtained maximum silencing fold for *gltA*, *pgi*, and *ppc* was as follows:

$$[\theta_M]^{gltA}_{P_{Ltac}(+)} \approx 6.6; \quad [\theta_M]^{pgi}_{P_{Ltac}(+)} \approx 10.8; \quad [\theta_M]^{ppc}_{P_{Ltac}(+)} > 100$$

It was reported previously[30] that the application of an alternative approach, namely, the paired-terminus antisense RNA (PTasRNA)-based strategy, when the P_{trc} promoter was used for *trans*-asRNA accumulation for the same genes, resulted in the following silencing efficiencies:

$$[\theta_M]^{gltA} \approx 12.5; \quad [\theta_M]^{pgi} \approx 20.0; \quad [\theta_M]^{ppc} \geq 2.7$$

Generally, the silencing folds obtained in the present study could be considered an attractive alternative to this approach. A 2-fold increased efficiency for the late approach in silencing *gltA* and *pgi* genes might not be critical because absolute residual activity of the corresponding enzymes was already very low.

Indeed, although achievement of the minimal enzyme activity by gene silencing was usually preferable for metabolic engineering, it was not always necessary. As reported, no more than a 50% decrease in the activity of the Pfk-I target was sufficient for significant redistribution of the desirable fluxes from a central *E. coli* metabolism.[38] Additionally, some methods for the possible enhancement of the silencing efficiency in CT-based silencing strategies are discussed in the Conclusions section.

Note that the design of the actuators constructed and tested in the current study allows them to be easily combined via classical P1*vir* transduction of their nonfunctional but Cm^R progenitors followed by λXis/Int-dependent curing of the marker, resulting in actuator activation in the new strain. To test the robustness of the approach and the possibility of efficient silencing of several genes simultaneously, the Cm^R progenitors of the strongest actuators *gltA*(R1.1)<P_{Ltac} and *pgi*(R1.1)<P_{Ltac} were transduced in the *ppc*(R1.1)<P_{tac} strain, followed by marker curing (Methods). Therefore, a new recombinant strain was obtained in which all three tested genes were silenced, in addition to the earlier obtained group in which single silenced mutants were present.

The experimental conditions for silencing detection were the same as those in the experiments with single mutants. As expected, the presence of an active actuator in one GOI resulted in some changes in the native expression rate of another GOI (see the GltA activity in the case of *pgi*(R1.1)<P_{Ltac}(+) and *ppc*(R1.1)<P_{tac}(+) in Figure S2), because of the metabolic response. A direct comparison of the silencing fold for the triple mutant with those of the corresponding single mutant strains revealed small differences related to the above-mentioned changes in the native expression of GOIs. However, this difference expectedly decreased with increasing actuator

https://dx.doi.org/10.1021/acssynbio.9b00463
ACS Synth. Biol. 2020, 9, 1650−1664

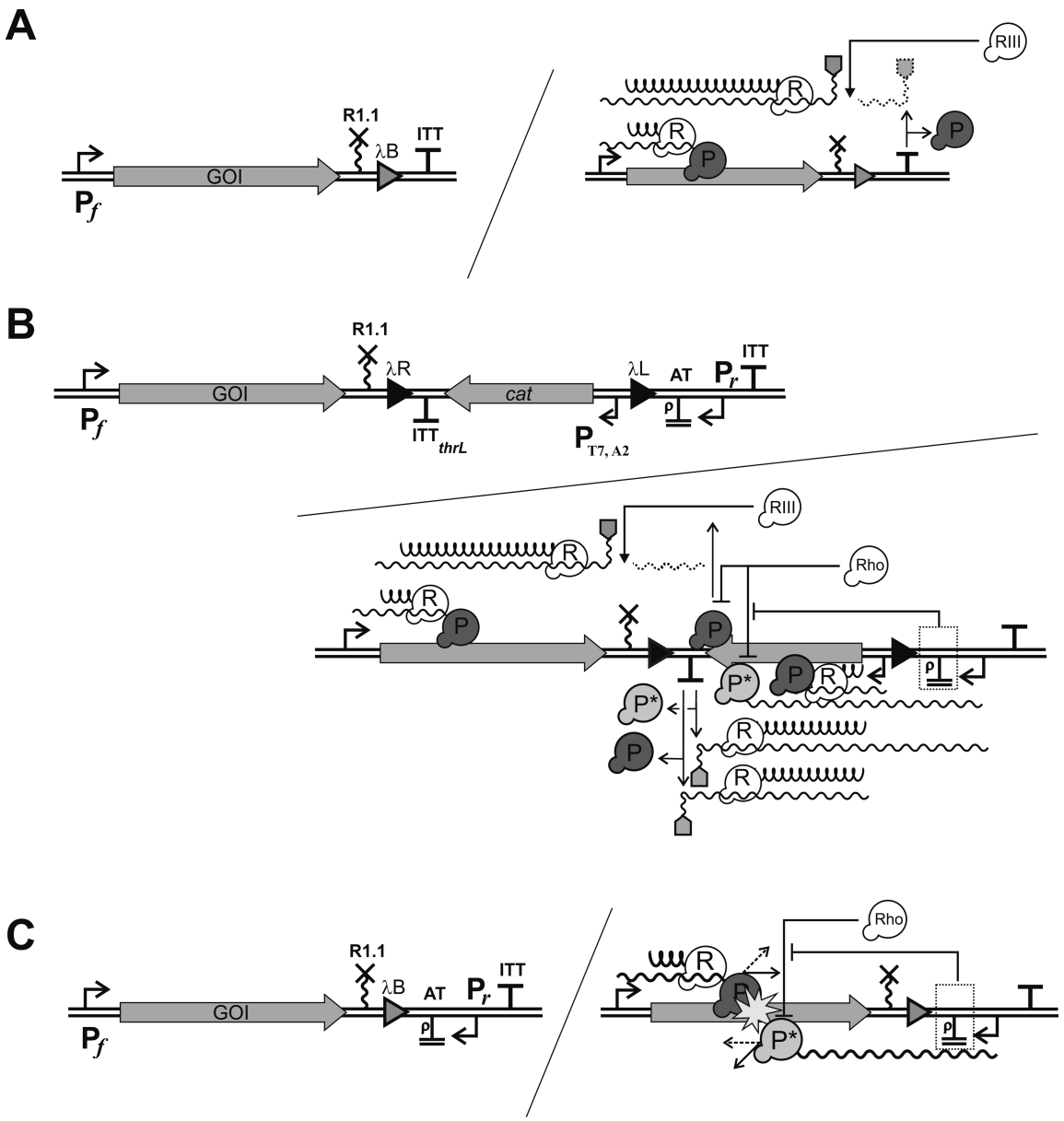

Figure 3. Structural and functional maps of three group mutant strains. Schemes for the strains (A) with only the R1.1 site at the 3′-UTR of the GOIs, (B) with an inactive actuator due to the presence of an excisable Cm^R marker with ITT_{thrL}, and (C) a fully functional constitutive actuator are shown. The proposed action scheme of related components is shown without possible interaction between *cis*-asRNA and mRNA. Abbreviations: RNAPs sensitive (P) and resistant to RhoTT (P*); ribosome (R); RNase III (RIII); Rho-factor (Rho); λ phage recombination sites (λR, λL, and λB); R1.1 RNase III-mediated processing site (R1.1); *rrnG* ribosomal antitermination-inducing sequence (AT); native promoter of GOI (P_f) and *r*-promoter (P_r); intrinsic transcription terminator (ITT). The scheme is correct for the *gltA* and *ppc* cases and partially for the *pgi* case because of the ITT_{pgi} deletion.

strength (with IPTG addition). Thus, the approach is robust, and the efficiency of the target gene actuator-based silencing practically does not decrease, even when several strong actuators were added for silencing other genes.

The unique feature of the CT-based silencing strategy implemented previously[25] and repeated again in the present study was the exploitation of the *r*-RNAP-mediated elongation complex that is resistant to RhoTT for the prevention of the untimely termination of nascent nontranslated asRNA. Recently, the negative effect of such termination was experimentally demonstrated for silencing by CT.[19] It was suggested[25] that after the generation of the *rrnG*-AT sequence in the 5′-terminus of the nascent RNA by *r*-RNAP, the elongation complex became resistant to RhoTT and continued transcription at a rate ≈85 nt/s, which is typical not for mRNA but for the synthesis of *E. coli* rRNA.[39] According to our knowledge, other authors who also applied CT-based silencing did not use the conversion of *r*-RNAP to the RhoTT resistant state.[16,15,22] To evaluate the influence of potential RhoTT on the silencing efficiency, a single nucleotide mutation, boxA-6UG, which disrupted the antitermination effect *in vivo*,[40] was introduced into the *rrnG*-AT boxA sequence of the actuator in the *pgi*(R1.1)<P_{Ltac} mutant. The following measurements revealed a decrease in the silencing fold $[\theta_M]^{pgi}_{P_{Ltac}(-/+)}$ = [(1.5)/(5.7)] in the strain with the mutant boxA in comparison with silencing fold $[\theta_M]^{pgi}_{P_{Ltac}(-/+)}$ = [(2.3)/(9.5)]

https://dx.doi.org/10.1021/acssynbio.9b00463
ACS Synth. Biol. 2020, 9, 1650−1664

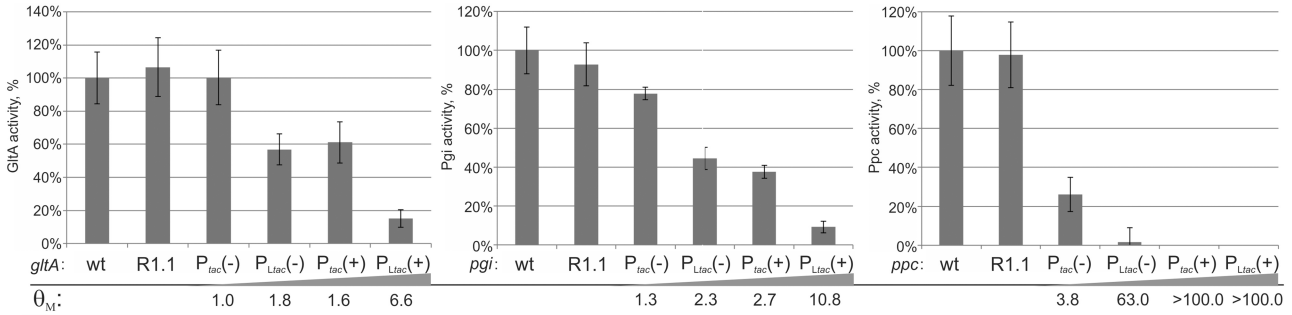

Figure 4. Residual steady-state activity of the targeted enzymes in the case of single-gene silencing. The calculated average silencing folds, θ_M, are shown below the corresponding columns. The standard deviation of three replications is indicated with error bars.

for the case of the actuator with a functional *rrnG*-AT sequence (Figure 5).

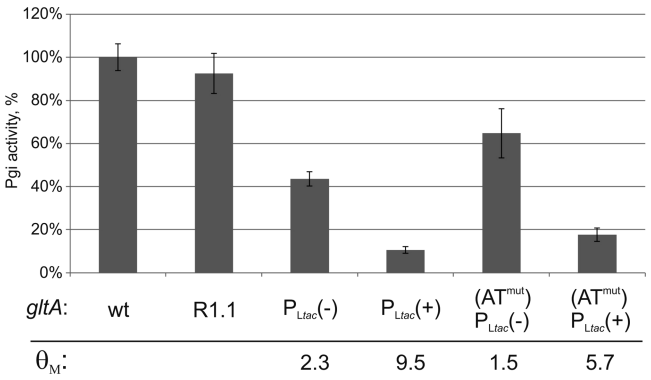

Figure 5. Residual steady-state activity of the *pgi* gene product in the case of active/inactive *rrnG*-AT. The experimentally measured silencing folds, θ_M, are shown below the corresponding columns. The standard deviation of three replications is indicated with error bars.

In full agreement with the previous proposal,[25] the presence of an active ribosomal antitermination-inducing sequence was even more important for the weaker *r*-promoters than for the stronger promoters (mutation in boxA restored over 20% of Pgi activity for $P_{Ltac}(-)$ and only 10% for $P_{Ltac}(+)$).

Although the boxA sequence alone may be sufficient for antitermination,[41] the use of a full-sized fragment of *rrnG*-AT, including boxA and boxB sequences,[26] is strongly recommended to maintain actuator robustness. Indeed, after fusion with any other *r*-promoter, in the case of a full-sized ribosomal antitermination-inducing sequence, an inherent upstream RNA hairpin structure of the boxB part will protect the downstream boxA in the nonstructured RNA form (Figure 1B), which is essential for contact with the NusB-NusE heterodimer during antitermination elongation complex formation.[42]

Two possible explanations for the positive influence of *rrnG*-AT on CT-mediated silencing are suggested. The protection of *r*-RNAPs from RhoTT resulted in (*i*) the accumulation of elevated amounts of asRNA that could interact with mRNA and (*ii*) an increase in the number of *r*-RNAPs that could participate in TI. Moreover, it could be additionally suggested that *r*-RNAP protected from RhoTT became a greater roadblock in head-on collisions with *f*-RNAPs than non-protected *r*-RNAP.

Analysis of the Obtained Results by Earlier Developed Simplified CT-Based Model. Currently, several mathematical models have been developed and applied for the description and explanation of CT-based silencing *in vivo*.[15,18,23,24] These models varied in complexity, modeling approach (e.g., stochastic simulation model, analytic models and models based on differential equations), experimental designs, and obtained data that were utilized to adjust optimal values for the model parameters. The best models predicted some mechanistic details about interference between elongating *f*-RNAP with trailing ribosome and converging *r*-RNAP generating *cis*-asRNA in a sensitive to RhoTT manner. In those experiments, the *f*-RNAPs survived in (85−93)% of their head-on collisions and continued the transcription[15,19] that finally resulted in rather low efficiency of GOIs silencing per one act of convergent collision.

The general design of the CT-based experiment was changed in the current study, mainly, due to conversion of *r*-RNAP-based elongation complexes in the RhoTT resistant state. As a result, the visible positive effect on silencing efficiency was obtained. It was interesting to evaluate quantitatively how this new design would influence the estimated parameters previously developed by Brophy and Voigt[15] with the mathematical model adjusted for the accomplished experimental modifications.

According to the chosen model, the GOI is silenced exclusively due to TI based on head-on collisions between converging *f*- and *r*-RNAPs, and polymerases may dissociate from the DNA in each collision.

As a reminder, the model consisted of the following elements: (i) the GOI (with a length L, [nt]) that is expressed due to mRNA (*f*-RNA) transcription coupled with translation; *f*-RNA synthesis is initiated from the P_f -promoter (fired with ϕ_f strength, [s^{-1}]), and the transcription elongation rate is v_f, [nt/s], (ii) the same GOI is transcribed in the reverse direction from P_r promoter (fired with ϕ_r strength, [s^{-1}]); the distance N, [nt], between transcription start points of face-to-face oriented promoters is approximately equal to a length of GOI; the asRNA (*r*-RNA) is generated with the elongation rate v_r, [nt/s], that is not equal to v_f due to the presence of the *rrnG*-AT sequence (Figure 6). The appearance of this sequence in the 5′-UTR of the nascent *r*-RNA induces conversion of *r*-RNAP in the state resistant to RhoTT and increases the elongation *r*-RNA transcription rate up to a value typical for the transcription rate of *E. coli* rRNA. The values of the mentioned above input model parameters had to be taken according to the literature and experimental data (Table S1).

One of the main features of the known CT models was the proposed fate of converging RNAPs after collision. Usually, authors assume that upon head-on collision, no more than

https://dx.doi.org/10.1021/acssynbio.9b00463
ACS Synth. Biol. 2020, 9, 1650−1664

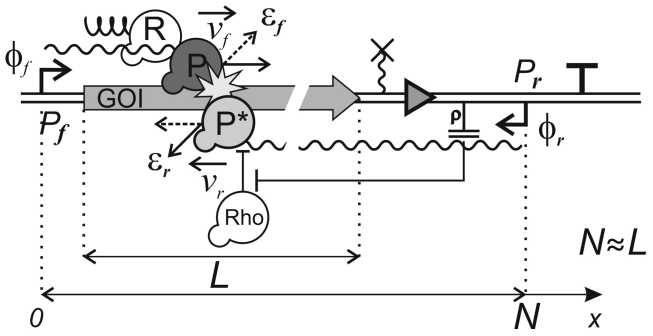

Figure 6. CT-based model of GOI silencing used in the current study. Only head-on collisions between converging *f*- and *r*-RNAPs (fired from the P_f and P_r promoter with ϕ_f [s^{-1}] and ϕ_r [s^{-1}] strength, and transcribed from the corresponding RNAs with the elongation rates v_f and v_r, respectively) were considered as the cause of GOI silencing. The scheme was not drawn to scale, and actually, the distance between transcription start points of face-to-face promoters, N [nt], was practically the same as the length of the ORF_{GOI}, L [nt], that is, $L \approx N$. The colliding elongation complexes were not equivalent: *f*-RNAP had a trailing ribosome; *r*-RNAP, in turn, was resistant to RhoTT. Polymerases from the both complexes could dissociate from the DNA in each collision with the probabilities ε_f and ε_r for *f*-RNAP and *r*-RNAP, respectively. These probabilities, ε_f and ε_r, initially were considered as free and independent parameters. Finally, the model was modified due to the addition of the constraint ($\varepsilon_f + \varepsilon_r = 1$) implicated with the proposal that only one from two collided RNAPs could continue transcription after each head-on collision.

one[16] or only one of the two colliding RNAPs[19] continues transcription. The simple assumption that both transcribing RNAPs never survive head-on collisions[18] has already been rejected because of its poor fit to experimental data.[15,43] In the current study, following the chosen model,[15] the most general assumption was initially used that each colliding RNAP could sometimes pass by each other and continue transcription without dissociation from the template. Therefore, it was assumed that each collided RNAP had independent probabilities to dissociate from the DNA template after collision, and they were named ε_f and ε_r for *f*-RNAPs and *r*-RNAPs, respectively, (Figure 6). Thus, the ε_f and ε_r probabilities were considered initially as free and independent parameters of the current model and denoted: $\varepsilon_f \in [0,1]$ and $\varepsilon_r \in [0,1]$.

According to the model, $C_f(x)$ and $C_r(x)$ are two real-valued functions, that denote steady-state concentrations of *f*-RNAP (C_f) and *r*-RNAP (C_r) at a given DNA site, with the argument x corresponds to the distance between the current site and the transcription initiation site of the P_f-promoter (Figure 6). Thus, CT can be described by a system of differential equations (special case of general Lotka-Volterra equations) with determined boundary conditions (Methods).

For the given pair of values for ε_f and ε_r, as free parameters, the system of equations could be numerically solved and the predicted silencing fold $\theta_P(\varepsilon_f, \varepsilon_r)$ could be calculated as the ratio of full-length ($x = N$) transcripts produced from the P_f-promoter without any collisions (i.e., without any dissociation of *f*-RNAPs from the DNA template, the $\varepsilon_f = 0$ case) and after collisions with elongation complexes initiating from the P_r-promoter (i.e., with possible dissociation of *f*-RNAPs, the $\varepsilon_f > 0$ case):

$$\theta_P(\varepsilon_f, \varepsilon_r) = \frac{C_f(x = N)|\varepsilon_f = 0}{C_f(x = N)|\varepsilon_f > 0}$$

In this study we used a modification of the parameter sweeping procedure used in ref 15 for each P_f- and P_r-promoter combination to solve the regression analysis problem and find the estimated values of the ε_f and ε_r parameters, ε_f^K and ε_r^K, respectively (since later in this study, estimates of the ε parameters from different studies are compared, the superscript letter is selected as the first letter of the first author of the study). This resulted in the best agreement between predicted θ_P and experimentally measured θ_M silencing folds with available experimental data. The sense of the modified procedure is briefly described in Methods.

For each promoter pair, the provided estimation of free parameters (and its validation with absolute relative error heatmaps, see Methods) unambiguously resulted in unique estimated values ε_f^K of ε_f parameter dispersed for different promoter pairs in the range $\varepsilon_f^K \in [0.14, 0.36]$. Surprisingly, the estimated value ε_r^K of the ε_r parameter was uniformly distributed in the range [0, 1] for each promoter pair, (i.e., a practically linear zone of the optimal estimated values of the ε_r on the corresponding heatmap (reliable data, Figure 7; all data, Figure S3).

It was impossible to unambiguously determine the ε_r parameter in the scope of the assumed model and available experimental data because of the structure of the parameter space which can be explained from a mathematical point of view by the mismatch between the number of independently estimated free parameters and the number of independently measured variables. Multiple optimal values of the ε_r parameter were based on the absence of a measured parameter that is directly connected with the fate of *r*-RNAPs, such as the enzymatic activity for the protein product of *f*-transcription for the ε_f parameter. The level of the full-sized *r*-RNA which was not experimentally measured in the current study, perhaps, could be applied for the single-valued determination of the ε_r parameter.

Thus, according to our knowledge, the problem of precisely determining both ε parameters simultaneously could be solved by either obtaining and using additional experimental data or by conceptual modification of the initial model due to the introduction of specific constraints/relationships between the ε_f and ε_r parameters.

Note that in the recent stochastic CT model designed in ref 19 it was proposed that only one of two colliding RNAPs continued transcription. The estimates of dissociation probabilities for *f*-/*r*-RNAPs were calculated with the addition of the following constraint: $\varepsilon_f^H + \varepsilon_r^H = 1$. An optimal value of the unique free model parameter was estimated as $\varepsilon_f^H \approx 0.07$, and therefore, the second value was calculated as $\varepsilon_r^H \approx 0.93$. Moreover, it was reported in ref 19 that the addition of the RNAP bypass possibility in their stochastic model did not improve convergence of the existing experimental data with the predicted silencing in the computational parameter optimization procedure. Indeed, although collision bypass could not be completely excluded from the theoretical point of view, it was experimentally shown only *in vitro* for single-subunit bacteriophage T7 and T3 RNAPs.[44] At the same time, *in vitro* studies with multisubunit prokaryotic[45] and eukaryotic[46] RNAPs suggested that their counterparts were not able to bypass each other. Moreover, *in vivo*, T7 RNAPs could not be fully "transparent" for *E. coli* RNAPs, and substantial TI could be detected for both types of colliding polymerases.[22]

Therefore, it seemed reasonable to include the above-mentioned constraint that only one of the two converging

https://dx.doi.org/10.1021/acssynbio.9b00463
ACS Synth. Biol. 2020, 9, 1650−1664

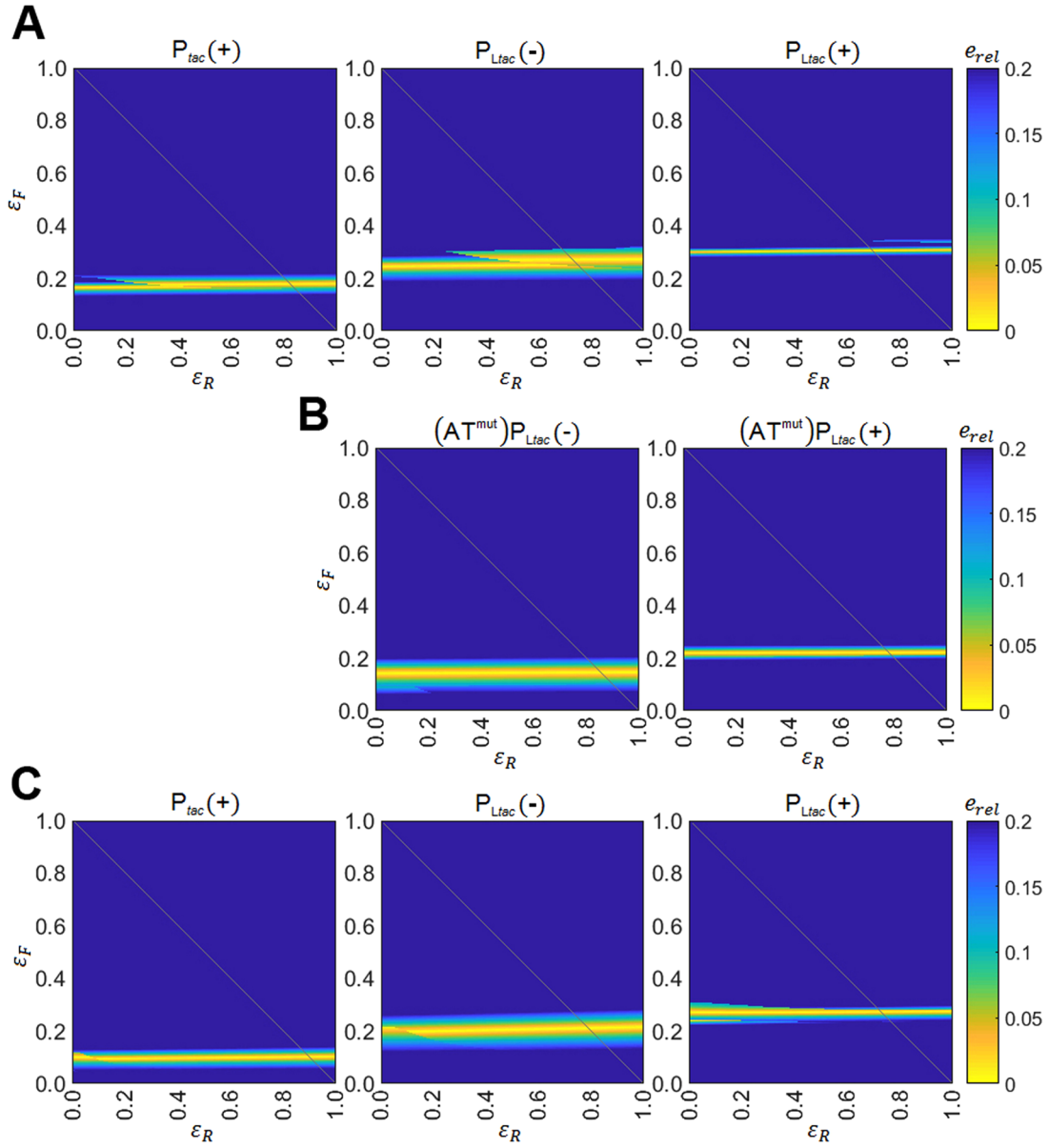

Figure 7. Parameter sweeping heatmaps. The most reliable heatmaps (A) for *pgi* silencing, (B) *pgi* in the case of the P_{Ltac} promoter fused with inactivated ribosomal antitermination-inducing sequence *rrnG*-AT and (C) *gltA* are shown. Each set of heatmaps contains values of absolute relative error, e_{rel}, between the predicted θ_P and measured θ_M silencing folds of the selected gene under *r*-promoter strengths P_{tac}(+), P_{Ltac}(−), and P_{Ltac}(+) calculated for different combinations of ε values. The *f* and *r* indexes of ε values denote dissociation probabilities of *f*-RNAPs and *r*-RNAPs, respectively. Light yellow indicates regions that demonstrate the best consensus between model-simulated and experimentally measured interference. The gray diagonal line represents the graphical solution of the $(\varepsilon_f + \varepsilon_r = 1)$ equation.

RNAPs would survive and continue transcription after head-on collision, that is, to add $(\varepsilon_f + \varepsilon_r = 1)$ in the assumed differential equations-based model. This assumption resulted in a unique estimated value ε_r^K of the ε_r parameter in each of the analyzed experiments in addition to already estimated ε_f^K. Thus, estimated values of the ε_r parameter belonged to the following range: $\varepsilon_r^K \in [0.64,0.86]$.

It should be noted, that a direct dependence of ε_f^K on the strength of the *r*-promoter was observed in all our data. According to the physical sense of ε_f, this result could be explained by only extreme simplification of the model to one that accounts for only collisional contribution to the general silencing fold value θ_M. No other mechanisms of TI and *cis*-asRNA-mRNA interactions were included in the model. Therefore, it seemed that the most reliable estimates of ε_f^K by the model were obtained under conditions of minimal P_r promoter strength and minimal GOI length. Indeed, reduced P_r promoter strength minimized the effect of promoter occlusion and sitting ducks in TI[18] and, on the other hand, decreased the quantity of generated *cis*-asRNAs; a reduced GOI length, in turn, certainly led to a decreased chance of the development of features for asRNA−mRNA interactions.[15]

Considering these factors, the most reliable parameters finally estimated in the current study were $\varepsilon_f^K \in [0.15, 0.25]$ and $\varepsilon_r^K \in [0.75, 0.85]$ for those experiments where *r*-RNAPs were resistant to RhoTT. However, in one experimental design of the current study, the resistance of the *r*-RNAP-based complex was disrupted by mutation in the *rrnG*-AT sequence of the actuator.[40] This disruption probably had to be accompanied by a decrease in *r*-transcription elongation rate

https://dx.doi.org/10.1021/acssynbio.9b00463
ACS Synth. Biol. 2020, 9, 1650−1664

from the value typical for rRNA up to the rate for mRNA synthesis. The estimation of ε_f and ε_r values for this experiment that was performed according to the standard parameter sweeping procedure with the addition of constrained ε_r parameter estimates resulted in $\varepsilon_f^{K*} \approx 0.12$ and $\varepsilon_r^{K*} \approx 0.88$, where the asterisk symbol (∗) in the superscript of $\varepsilon_{f/r}$ values means that the value was specific for the currently studied states of colliding elongation complexes.

It was interesting to compare the probabilities $\varepsilon_{f/r}$ and the bias between their values estimated for the elongation complexes with that of RNAP in the previous[19] and in the present study (Table 2). Both studies assumed the same

Table 2. Dissociation Probabilities of *f*- and *r*-RNAPs during Their Collisions Estimated in Different Studies[a]

state of *f*-RNAPs/ state of *r*-RNAPs	ε_f	ε_r	bias = $\varepsilon_r/\varepsilon_f$	ref
(Tr+, RhoTT^S)/ (Tr-, RhoTT^R)	[0.15, 0.25]	[0.75, 0.85]	[3.0, 5.7]	this study
(Tr+, RhoTT^S)/ (Tr-, RhoTT^S)	0.12	0.88	7.3	this study
	0.07	0.93	13.3	19

[a]RNAP elongation complexes generating RNA were with/without trailing ribosomes (Tr+/Tr-) and were either sensitive (RhoTT^S) or resistant (RhoTT^R) to RhoTT.

mechanistic result of collision for convergent RNAPs that only one continue the transcription, but colliding elongation complexes were not completely the same. Indeed, *f*-RNAP- or *r*-RNAP-based complexes generating mRNA or asRNA were with or without trailing ribosomes (Tr+ or Tr-, respectively) and were either sensitive (RhoTT^S) or resistant (RhoTT^R) to RhoTT.

The presented results confirmed the previously established[15,19] fact that *f*-RNAP with a trailing ribosome had a significantly higher probability of surviving and continuing transcription after a head-on collision than untrailed *r*-RNAP, which is sensitive to RhoTT. However, the application of an actuator constructed according to the new design decreased this bias by a minimum of several-fold due to the transfer of *r*-transcription into a state that is resistant to potential termination and thus increased the efficiency of the standard CT-based gene silencing.

CONCLUSIONS

In the present study, the improved universal constitutive actuator providing CT-based silencing of GOIs was tested for three typical metabolic *E. coli* genes, *pgi*, *gltA*, and *ppc*. For the P_r promoters for CT, the O_{lac}-carrier promoters P_{tac} and P_{Ltac} were used in constitutive mode (with/without IPTG addition) with four step-different initiation transcription rates. The strengths of the *r*-promoters were greater than those of the *f*-promoters of the selected GOIs within all tested ranges. Indeed, even the weakest *r*-promoter, $P_{tac}(-)$, was 3-fold stronger than the strongest *f*-promoter, P_{ppc}. It was not surprising that the high bias in *r*-promoter strength over their *f*-counterparts in CT resulted in highly efficient silencing in all tested cases. The previously established dependence of the efficiency of silencing on the *r*-promoter strength and GOI length was expectedly confirmed. The main feature of the CT design used in the present study was the application of the specifically and previously developed[25] actuator composed of the *E. coli* ribosomal antitermination-inducing sequence *rrnG*-AT fused to the *r*-promoter. The corresponding actuator design could help protect the transcribing *r*-RNAPs from the potential RhoTT and retain them at the DNA template for collision with *f*-RNAPs and, finally, increase the silencing efficiency. Moreover, insertion of the R1.1 RNase III processing site instead of ITT_{GOI}, as a part of the developed robust actuator in the current study, did not significantly change the native expression level of the tested GOIs and excluded the possible negative impact on silencing fold by potential bidirectional ITT of *r*-transcription before the converging region.

The silencing fold achieved by the developed actuator correlated well with the data obtained by other authors using relatively more sophisticated and highly specific approaches. However, it could be challenging to achieve efficient silencing in the case of a GOI shorter than the tested GOIs. It seems that the tested approach could be effective for GOIs with a length of approximately 1 kb (the average ORF size of *E. coli* is 317 aa[47]), according to rather limited previously published data.[15]

So, only a rather short GOI could limit application of the supposed silencing strategy. In that case, increasing the CT length with a serious modification of the GOI structure could be performed. It is possible to create an artificial operon for which the full-sized structural part of GOI would be used as a distal gene. The proximal gene would be the N-terminal part of ORF_{GOI} fused in-frame with one from several artificial ORFs located in the middle of the operon and arranged similar to the *λP-Q*(ninR) region.[48] The latter contains a series of ORFs with partially overlapped terminator (TGA) and (re)initiator (ATG) codons and with the location of the putative SD sequence of each distal ORF in the coding part of its proximal partner. The proposed structure of the so-called "overlapon"[49] could retain the expression activity of the initial GOI due to the transcription/translation coupling effect, according to the previously developed approach,[50] and at the same time significantly increase the effective target length between the convergent promoters for CT-based silencing.

In the context of the definitively determined molecular mechanisms, the obtained silencing effects were significantly simplified in the model applied in the current study, where only collisions between elongating convergent RNAPs were included. Nevertheless, this simplified approach could help obtain the parameters characterized by the differences in the stabilities of the elongation complexes of *f*-/*r*-RNAPs with a DNA template in the process of head-on collision, which would logically correspond to the data obtained by other authors using analogous experimental models. Broadening the statistics (using tested GOIs with different structural features and lengths) of the corresponding experiments could help to improve the applied model by introducing the influence of all possible TI factors and specific features of *cis*-asRNA−mRNA interactions on the final effect of GOI silencing.

METHODS

Strains and Media. *E. coli* MG1655 (F$^-$, *λ*$^-$, *ilvG*$^-$, *rfb50*, *rph*$^-$) and CC118 (Δ(*ara-leu*), *araD*, Δ*lacX74*, *galE*, *galK*, *phoA20*, *thi-1*, *rpsE*, *rpoB*, *argE* (Am), *recA1*, *λpir* phage lysogen) and its corresponding derivative mutant were used (Table 1).

Cells were grown in either LB (Miller) for routine cultivation or in SOB/SOC medium for electroporation procedures or M9 minimal medium[51] supplemented with

https://dx.doi.org/10.1021/acssynbio.9b00463
ACS Synth. Biol. 2020, 9, 1650−1664

0.4% glucose. IPTG was used at a final concentration of 0.5 mM. Antibiotics were used at the following concentrations: chloramphenicol (Cm), 30 μg/mL; ampicillin (Ap), 100 μg/mL; tetracycline (Tc), 12.5 μg/mL.

Experimental Strain Construction. Strains in which the genes *gltA*, *pgi*, and *ppc* were silenced by CT with the P_{tac} and P_{Ltac} *r*-promoters and the corresponding control strains with the insertion of only the RNase III processing site R1.1 at the 3′-end of the mentioned genes were constructed from the *E. coli* MG1655 strain by λRed-mediated recombination[52] (Figure S4) by using corresponding oligonucleotides (Table S2). Because of the design, the actuator becomes active only after the elimination of the chloramphenicol resistance marker (Cm^R). Thus, the construction of experimental strains (Table 1) was finished after the Cm^R marker excision by λXis/Int-mediated site-specific recombination[53] and the formation of a scar sequence (Figure 1A).

Notably, the upstream part of the artificial P_{Ltac} promoter (Figure 1C) is a part of the λP_L promoter (from 35 620 and up to 35 710 according to the λ genome NC001416; Figure S5), and the downstream part is part of the well-known P_{tac} promoter (from −36 and up to +22). The activity of P_{Ltac} is partially repressed by the LacI repressor due to the presence of O_{lac} located as it is in P_{tac} (from +1 to +21) and by the λCI repressor that can interact with O_L2 and O_L3 cooperatively in their native positions in the absence of O_L1. The presence of the AT-rich UP element and the integration host factor (IHF)-binding site in the structure of P_{Ltac} explains the increased strength of this promoter over P_{tac} in IHF^+ cells without the λCI repressor.

For the construction of a single strain with simultaneous triple gene silencing, target genes from uncured Cm^R donor strains, *pgi*(R1.1)<P_{Ltac} and *gltA*(R1.1)<P_{Ltac}, were transferred with subsequent marker elimination in two steps by the P1*vir* transduction procedure[51] into the markerless recipient strain *ppc*(R1.1)<P_{tac}.

To accurately estimate promoter strength, an integrative plasmid named pAHZG containing a promoter-less reporter gene encoding the ZsGreen protein[54] was constructed on the basis of the integrative plasmid pAH162-λ*attL*-TcR-λ*attR*[55] (Figure S6). The RNase III processing site R1.1 was applied as an insulator in pAHZG to eliminate the influence of different 5′-UTRs that come from different 3′-end promoter sequences on $mRNA_{zsgreen}$ and *zsgreen* translation, as was previously performed for pTL61.[56]

Second, the promoters of interest, P_{pgi}, P_{ppc}, P_{gltA}, P_{tac}, and P_{Ltac}, were PCR-amplified with corresponding oligonucleotides (Table S2) and cloned into the pAHZG plasmid to obtain the plasmids pAHZG-P_x, where P_x represents some of the promoters described in this study (Figure S7). The plasmid pAHZG-λP_L was constructed previously in the same way and was taken from a laboratory stock collection.

Finally, each of the pAHZG-P_x plasmids was individually integrated into the native ϕ80*attB* site (located in the *yciI* gene (1 310 413−1 310 761 according to MG1655 genome NC 000913.3) strain by the Dual In/Out strategy.[55] Elimination of the tetracycline resistance (Tc^R) marker and plasmid replicon from the chromosome of the obtained integrant strains by λXis/Int-mediated site-specific recombination completed the construction of P_x-zsg strains (Table 1).

Promoter Strength Estimation. Estimation of the promoter strength was performed by a fluorescence assay. P_x-zsg strains with different P_x-*zsgreen* cassettes integrated into thier chromosomes were grown overnight in minimal M9 glucose-supplemented medium at 37 °C. Then, the overnight culture was diluted to OD = 0.025 in the same fresh medium not supplemented or supplemented with 0.5 mM IPTG and continued to grow at 37 °C. Samples were taken each hour. The OD (at 600 nm) and fluorescence, *F* (excitation at 490 nm and emission at 530 nm), were measured with an Infinite M200 PRO plate reader (Tecan Group Ltd., Swiss). Promoter activity was calculated as described in Leveau et al.[57] by the following equation:

$$P = \left(\frac{\delta F_{\text{sample}}}{\delta \text{OD}_{\text{sample}}} - \frac{\delta F_{\text{control}}}{\delta \text{OD}_{\text{control}}}\right)\mu\left(1 - \frac{\mu}{m}\right)$$

where μ is the growth rate (per hour) and *m* is the maturation time constant (per hour) and the control strain was MG1655 with an integrated promoter-less *zsgreen* cassette, *yciI*::*zsgreen*. The resulting promoter activity *P* for each promoter of interest was normalized by the *P* calculated for the λP_L promoter and used to estimate absolute transcriptional strength.

The absolute transcriptional strength of promoters was calculated in terms of transcr/s. Briefly, investigators from the laboratory of Prof. H. Bujard precisely measured the relative and estimated absolute promoter strength for the group of strong promoters[31] recognized by *E. coli* RNAP with the σ^{70}-subunit (RNAP-σ^{70}) that synthesize mRNA with an average elongation rate ≈(40−50) nt/s.[58] Accordingly, assuming that the space requirement of the ≈50 bp DNA/1 molecule of RNAP in the promoter complex and the promoter clearance rate is the same as the elongation rate, it was proposed that the strongest promoter (tandem ribosomal promoters) could manifest activity of ∼1 transcr/s in an excess of free RNAP in the cell, which was approximately estimated as 100-fold greater than the measured strength of the P_{bla} promoter[59] with only ∼2-fold higher activity than the activity of the λP_L variant promoter used in the same report (called $\lambda P_{L,\ Deuschle}$ in our study (Figure S5)); this was determined, in turn, as ≈0.50 transcr/s. Another independent estimation of λP_L promoter strength *in vivo* was performed by Liang et al.,[32] and it was approximately 17 transcr/min (∼0.28 transcr/s) in the fast-growing cells used in the same report as for the λP_L variant (called $\lambda P_{L,\ Liang}$ in our study (Figure S5)). Considering that the relative strengths of the different truncated variants of λP_L significantly depend on their structure[33] (Figure S5), the re-evaluated promoter strength for the full-sized λP_L that was used in the present study reached a maximum of 0.55 transcr/s according to Liang et al.[32] Thus, these two estimations provided very similar results, and it was assumed that variations based on the intracellular concentration of free RNAP, cellular growth rate, and location of the promoter at different points might be included within the mentioned interval ≈ (0.50−0.55) transcr/s. Thus, considering the growth conditions of the experimental strains in the present study and in the above-mentioned two articles, the absolute transcriptional strength of the λP_L promoter was set as 0.5 transcr/s, and the same parameter for other promoters was calculated by multiplication of their relative strength to 0.5.

Silencing Measurement Experimental Procedure. For each individual experiment, strains were first inoculated on LB plates from −70 °C freezer stocks and grown overnight at 37 °C. Then, one 5 μL loop was seeded in 5 mL of liquid M9 minimal medium supplemented with 0.4% glucose and 0.05% thiamine and cultured overnight at 37 °C. Additionally, 5 mM

https://dx.doi.org/10.1021/acssynbio.9b00463
ACS Synth. Biol. 2020, 9, 1650−1664

L-aspartate was added to the same medium for the cultivation strain with the silenced *ppc* gene. The overnight culture for each strain was seeded into two 5 mL cultures of fresh liquid M9 minimal medium supplemented with 0.4% glucose and 0.05% thiamine and with/without 0.5 mM IPTG. The starting OD_{600} was approximately 0.025. New stable minimal concentrations of GltA, Pgi, and Ppc were achieved in 6, 5, and 5.5 h of growth, respectively. At that time, the OD_{600} was in the range of 0.5−0.8 depending on the strain and induction.

To confirm the chosen optimal sampling time and obtain detailed growth curves, the following protocol was applied twice for each experimental strain. Briefly, after 5−6 h of growth at 37 °C, the culture was diluted again to an OD_{600} of 0.025 in fresh medium of the same composition and allowed to continue overnight growth in a RVS062CA Compact Rocking Incubator (Advantec Toyo Seisakusho Kaisha Ltd., Japan) with automatic OD_{660} measurements every 15 min. The corresponding enzymatic activities were measured at the beginning and end of cultivation, which was 24 h after IPTG supplementation (where necessary), and confirmed that the maximal silencing was already achieved for all GOIs at 5−6 h (Figure S8).

***In Vitro* Enzyme Activity Assay.** All following operations were carried out on ice. Cells were washed twice with 0.9% NaCl. Then, they were resuspended in Buffer I, which had the following composition: 100 mM Tris-HCl, pH 7.5, 20 mM KCl, 2 mM DTT, and 0.5 mM EDTA. Then, cells were disrupted for 1.5 min by sonication in a Vibra-Cell (Sonics Sonics & Materials Inc., USA). Note that Buffer I did not contain DTT for the measurement of GltA activity. The cell debris was removed by centrifugation at 13 000*g* for 20 min at +4 °C. Supernatants were used for the determination of total protein and enzymatic activity. Total protein concentration was determined using the Protein Assay Dye Reagent (Bio-Rad Laboratories, Inc., USA) with bovine serum albumin standards in accordance with the manufacturer's instructions. Absorbance in all described cases was measured with a Synergy2 Microplate Reader (BioTek Instruments, Inc., USA).

Measurement of glucose-6-phosphate isomerase (Pgi) activity was based on the isomerization of D-fructose-6-phosphate into D-glucose-6-phosphate in a Pgi-catalyzed reaction, followed by the conversion of the product into D-glucono-1,5-lactone-6-phosphate (gluconolactone-6P).[60] $NADP^+$ utilization allowed the reaction to be monitored at 340 nm. The reaction buffer contained 100 mM Tris-HCl, pH 7.8, 5 mM $MgCl_2$, 2.5 mM D-fructose-6-phosphate, 0.5 mM $NADP^+$, 2 U/mL glucose-6-phosphate dehydrogenase, and 25 μg/mL total protein.

Citrate synthase (GltA) transfers the acetyl group from acetyl-CoA to oxaloacetate to produce deacetylated CoA and citrate. The appearance of free SH groups can be monitored by coloring with 5,5′-dithio-bis(2-nitrobenzoic acid) (DTNB, Ellman's reagent).[61] This reaction is easily evaluated at 414 nm, where the mercaptide ion (5-mercaptho-2-nitrobenzoate) has a strong absorption. The reaction buffer contained 100 mM Tris-HCl, pH 8.1, 0.5 mM oxaloacetate, 0.2 mM acetyl-CoA, 0.5 mM DTNB, and 50 μg/mL total protein.

Phosphoenolpyruvate carboxylase (Ppc) catalyzes the conversion of phosphoenolpyruvate into oxaloacetate through carbon dioxide fixation. The course of the reaction can easily be observed by the conversion of oxaloacetate into L-malate in an NADH-dependent manner with a malate dehydrogenase-catalyzed reaction, which was monitored at 340 nm.[62] The reaction buffer contained 100 mM Tris-HCl, pH 7.5, 4 mM DTT, 50 mM $NaHCO_3$, 5 mM $MnSO_4$, 4 U/mL malate dehydrogenase, 0.45 mM NADH, 5 mM PEP, 0.1 mM acetyl-CoA, and 50 μg/mL of total protein.

CT Model Calculations. As determined by Brophy and Voight,[15] collision interference can be described by the system of two differential equations for C_f and C_r functions representing steady-state concentrations of *f*- and *r*-RNAPs, respectively, at a site x, in which the argument x (in bp) corresponds to the distance from the start of the *f*-promoter:

$$\begin{cases} \dfrac{dC_f}{dx} = -\varepsilon_f C_f(x) C_r(x), \\ \dfrac{dC_r}{dx} = \varepsilon_r C_f(x) C_r(x), \end{cases}$$

where $\varepsilon_f \in [0, 1]$ and $\varepsilon_r \in [0, 1]$ are the probabilities of *f*- and *r*-RNAPs dissociating from the DNA template after a head-on collision, initially considered as free and independent parameters.

Boundary conditions for this system were defined by the rates of converging RNAPs that were initiated from the P_f-promoter, $C_f(x = 0) = \phi_f/v_f$, and the P_r-promoter, $C_r(x = N) = \phi_r/v_r$. The equations were numerically solved for each promoter pair combinations, and optimal ε parameters were selected that resulted in the best coincidence between predicted θ_P and experimentally measured θ_M silencing folds.

A brief description of this procedure and its validation follows. A MATLAB software-based procedure provided by Brophy and Voigt[15] was slightly modified to adjust the model to our experimental conditions. First, a discrete regular grid $G_\lambda = G_\lambda(\varepsilon_f, \varepsilon_r)$ of ε_f and ε_r parameter values was selected, with $(\varepsilon_f, \varepsilon_r) \in [0, 1] \times [0, 1]$, and the step λ of the grid was selected depending on the required precision of the estimated parameters (typically, $\lambda = 0.01$). Next, consensus between the measured silencing fold θ_M and predicted silencing θ_P was calculated for each grid point based on rectilinear distance. Formally, for each grid point, the following score value was assigned:

$$s = |\theta_M - \theta_P|^{-1}$$

Additionally, for each point of the grid G_λ, the value of the relative absolute error e_{rel} between the measured θ_M and predicted θ_P silencing fold was calculated:

$$e_{rel} = \frac{|\theta_M - \theta_P|}{\theta_M}$$

The best ε_f and ε_r were calculated as a weighted average of all the ε values of the grid, where the s score was used as the corresponding weight of the grid point. Finally, parameter sweeping was validated, because in certain cases, the regression problem could have multiple solutions (*e.g.*, complex parameter spaces with multiple sets of optimal and near-optimal sets of parameter values), and the use of averaging in parameter sweeping procedures could result in significant bias in the determination of the optimal values of the parameters. For these purposes heatmaps of absolute relative error e_{rel} values were constructed for each investigated promoter pair and all calculated pairs of optimized model parameter values ε_f and ε_r (Figure 7) to analyze the structure of the parameter space and validate the uniqueness of the acquired optimal parameter values.

https://dx.doi.org/10.1021/acssynbio.9b00463
ACS Synth. Biol. 2020, 9, 1650−1664

Furthermore, the following technical modifications were made to the scripts to increase numerical stability in model computations. The size of the differential equation solver's mesh was modified to be the parameter of the length of the gene ($\sigma_{bvp}N$, where σ_{bvp} is a scaling parameter that can be adjusted to balance precision and computational complexity). The numerical approximation of integration constants for the general solution of the model differential equations with the MATLAB FMINCON constraint solver was added as an alternative to the symbolic computation method when the license for the MATLAB's Symbolic Math Toolbox is absent. The source code of the adjusted model is provided in the Supporting Information.

■ ASSOCIATED CONTENT

Supporting Information

The Supporting Information is available free of charge at https://pubs.acs.org/doi/10.1021/acssynbio.9b00463.

Source code of the adjusted mathematical model (ZIP)

Growth kinetics of the model strains; residual steady-state activity of the targeted enzymes; parameter sweeping heatmaps; scheme and steps of the mutant strains. the pAHZG. and pAHZG-Px plasmid constructions; structure of the $\lambda P_L/O_L$ regulatory region; residual activity of enzymes for prolonged cultivation of mutant strains; input model parameters; oligonucleotides used in this study (PDF)

■ AUTHOR INFORMATION

Corresponding Author

Alexander A. Krylov − *Ajinomoto-Genetika Research Institute, Moscow 117545, Russian Federation*; orcid.org/0000-0003-1990-7385; Email: Alex_Krylov@agri.ru

Authors

Valeriya V. Shapovalova − *Ajinomoto-Genetika Research Institute, Moscow 117545, Russian Federation*

Elizaveta A. Miticheva − *Faculty of Biotechnology, Lomonosov Moscow State University, Moscow 119991, Russian Federation*

Mikhail S. Shupletsov − *Ajinomoto-Genetika Research Institute, Moscow 117545, Russian Federation; Faculty of Computational Mathematics and Cybernetics, Lomonosov Moscow State University, Moscow 119991, Russian Federation*

Sergey V. Mashko − *Ajinomoto-Genetika Research Institute, Moscow 117545, Russian Federation; Faculty of Biology, Lomonosov Moscow State University, Moscow 119991, Russian Federation*

Complete contact information is available at: https://pubs.acs.org/10.1021/acssynbio.9b00463

Notes

The authors declare no competing financial interest.

■ ABBREVIATIONS

asRNA, antisense RNA; CT, convergent transcription; *f-*, forward (promoters, RNAP etc.); GOI, gene of interest; IHF, integration host factor; ITT, intrinsic transcription terminator; *r-*, reverse (promoters, RNAP etc.); RhoTT, Rho-dependent transcription termination; RNAP, RNA polymerase; TI, transcriptional interference; UTR, untranslated region

■ REFERENCES

(1) Farmer, W. R., and Liao, J. C. (2000) Improving lycopene production in *Escherichia coli* by engineering metabolic control. *Nat. Biotechnol. 18*, 533−537.

(2) Holtz, W. J., and Keasling, J. D. (2010) Engineering static and dynamic control of synthetic pathways. *Cell 140*, 19−23.

(3) Tan, S. Z., and Prather, K. L. (2017) Dynamic pathway regulation: recent advances and methods of construction. *Curr. Opin. Chem. Biol. 41*, 28−35.

(4) Cameron, D. E., and Collins, J. J. (2014) Tunable protein degradation in bacteria. *Nat. Biotechnol. 32*, 1276−1281.

(5) Moser, F., Borujeni, A. E., Ghodasara, A. N., Cameron, E., Park, Y., and Voigt, C. A. (2018) Dynamic control of endogenous metabolism with combinatorial logic circuits. *Mol. Syst. Biol. 14*, e8605.

(6) McGinness, K. E., Baker, T. A., and Sauer, R. T. (2006) Engineering controllable protein degradation. *Mol. Cell 22*, 701−707.

(7) Wachsmuth, M., Findeiß, S., Weissheimer, N., Stadler, P. F., and Mörl, M. (2013) De novo design of a synthetic riboswitch that regulates transcription termination. *Nucleic Acids Res. 41*, 2541−2551.

(8) Gardner, T. S., Cantor, C. R., and Collins, J. J. (2000) Construction of a genetic toggle switch in *Escherichia coli*. *Nature 403*, 339−342.

(9) Politz, M. C., Copeland, M. F., and Pfleger, B. F. (2013) Artificial repressors for controlling gene expression in bacteria. *Chem. Commun. (Cambridge, U. K.) 49*, 4325−4327.

(10) Qi, L. S., Larson, M. H., Gilbert, L. A., Doudna, J. A., Weissman, J. S., Arkin, A. P., and Lim, W. A. (2013) Repurposing CRISPR as an RNA-guided platform for sequence-specific control of gene expression. *Cell 152*, 1173−1183.

(11) Nakashima, N., Goh, S., Good, L., and Tamura, T. (2012) Multiple-Gene Silencing Using Antisense RNAs in *Escherichia coli* in *Functional Genomics. Methods in Molecular Biology (Methods and Protocols)* (Kaufmann, M., and Klinger, C., Eds.) pp 307−319, Springer, New York.

(12) Tchurikov, N. A., Chistyakova, L. G., Zavilgelsky, G. B., Manukhov, I. V., Chernov, B. K., and Golova, Y. B. (2000) Gene-specific silencing by expression of parallel complementary RNA in *Escherichia coli*. *J. Biol. Chem. 275*, 26523−26529.

(13) Georg, J., and Hess, W. R. (2011) cis-antisense RNA, another level of gene regulation in bacteria. *Microbiol. Mol. Biol. Rev. 75*, 286−300.

(14) Shearwin, K. E., Callen, B. P., and Egan, J. B. (2005) Transcriptional interference − a crash course. *Trends Genet. 21*, 339−345.

(15) Brophy, J. A., and Voigt, C. A. (2016) Antisense transcription as a tool to tune gene expression. *Mol. Syst. Biol. 12*, 854.

(16) Bordoy, A. E., Varanasi, U. S., Courtney, C. M., and Chatterjee, A. (2016) Transcriptional interference in convergent promoters as a means for tunable gene expression. *ACS Synth. Biol. 5*, 1331−1341.

(17) Hao, N., Crooks, M. T., Palmer, A. C., Dodd, I. B., and Shearwin, K. E. (2019) RNA polymerase pausing at a protein roadblock can enhance transcriptional interference by promoter occlusion. *FEBS Lett. 593*, 903−917.

(18) Sneppen, K., Dodd, I. B., Shearwin, K. E., Palmer, A. C., Schubert, R. A., Callen, B. P., and Egan, J. B. (2005) A mathematical model for transcriptional interference by RNA polymerase traffic in *Escherichia coli*. *J. Mol. Biol. 346*, 399−409.

(19) Hoffmann, S. A., Hao, N., Shearwin, K. E., and Arndt, K. M. (2019) Characterizing transcriptional interference between converging genes in bacteria. *ACS Synth. Biol. 8*, 466−473.

(20) Ward, D., and Murray, N. E. (1979) Convergent transcription in bacteriophage λ: interference with gene expression. *J. Mol. Biol. 133*, 249−266.

(21) O'Connor, C D, and Timmis, K N (1987) Highly repressible expression system for cloning genes that specify potentially toxic proteins. *J. Bacteriol. 169*, 4457−4462.

(22) Hoffmann, S. A., Kruse, S. M., and Arndt, K. M. (2016) Long-range transcriptional interference in *E. coli* used to construct a dual

positive selection system for genetic switches. *Nucleic Acids Res. 44*, e95.
(23) Bordoy, A. E., and Chatterjee, A. (2015) Cis-antisense transcription gives rise to tunable genetic switch behavior: a mathematical modeling approach. *PLoS One 10*, No. e0133873.
(24) Hao, N., Palmer, A. C., Ahlgren-Berg, A., Shearwin, K. E., and Dodd, I. B. (2016) The role of repressor kinetics in relief of transcriptional interference between convergent promoters. *Nucleic Acids Res. 44*, 6625−6638.
(25) Krylov, A. A., Airich, L. G., Kiseleva, E. M., Minaeva, N. I., Biryukova, I. V., and Mashko, S. V. (2010) Conditional silencing of the *Escherichia coli pykF* gene results from artificial convergent transcription protected from Rho-dependent termination. *J. Mol. Microbiol. Biotechnol. 18*, 1−13.
(26) Albrechtsen, B., Ross, B. M., Squires, C., and Squires, C. L. (1991) Transcriptional termination sequence at the end of the *Escherichia coli* ribosomal RNA G operon: complex terminators and antitermination. *Nucleic Acids Res. 19*, 1845−1852.
(27) Dunn, J. J., and Studier, F. W. (1973) T7 early RNAs are generated by site-specific cleavages. *Proc. Natl. Acad. Sci. U. S. A. 70*, 1559−1563.
(28) Panayotatos, N., and Truong, K. (1985) Cleavage within an RNase III site can control mRNA stability and protein synthesis in vivo. *Nucleic Acids Res. 13*, 2227−2240.
(29) Naville, M., Ghuillot-Gaudeffroy, A., Marchais, A., and Gautheret, D. (2011) ARNold: a web tool for the prediction of Rho-independent transcription terminators. *RNA Biol. 8*, 11−13.
(30) Nakashima, N., Ohno, S., Yoshikawa, K., Shimizu, H., and Tamura, T. (2014) A vector library for silencing central carbon metabolism genes with antisense RNAs in *Escherichia coli*. *Appl. Environ. Microbiol. 80*, 564−573.
(31) Deuschle, U., Kammerer, W., Gentz, R., and Bujard, H. (1986) Promoters of *Escherichia coli*: a hierarchy of in vivo strength indicates alternate structures. *EMBO J. 5*, 2987−2994.
(32) Liang, S.-T., Bipatnath, M., Xu, Y.-C., Chen, S.-L., Dennis, P., Ehrenberg, M., and Bremer, H. (1999) Activities of constitutive promoters in *Escherichia coli*. *J. Mol. Biol. 292*, 19−37.
(33) Giladi, H., Koby, S., Prag, G., Engelhorn, M., Geiselmann, J., and Oppenheim, A. B. (1998) Participation of IHF and a distant UP element in the stimulation of the phage λPL promoter. *Mol. Microbiol. 30*, 443−451.
(34) Golding, I., Paulsson, J., Zawilski, S. M., and Cox, E. C. (2005) Real-time kinetics of gene activity in individual bacteria. *Cell 123*, 1025−1036.
(35) Gama-Castro, S., Salgado, H., Santos-Zavaleta, A., Ledezma-Tejeida, D., Muñiz-Rascado, L., García-Sotelo, J. S., et al. (2016) RegulonDB version 9.0: high-level integration of gene regulation, coexpression, motif clustering and beyond. *Nucleic Acids Res. 44*, D133−D143.
(36) Katashkina, Zh. I., Skorokhodova, A. Iu., Zimenkov, D. V., Gulevich, A. Iu., Minaeva, N. I., Doroshenko, V. G., Biriukova, I. V., and Mashko, S. V. (2005) Tuning of expression level of the genes of interest located in the bacterial chromosome. *Mol. Biol. (Moscow, Russ. Fed., Engl. Ed.) 39*, 823−831.
(37) Christodoulou, D., Link, H., Fuhrer, T., Kochanowski, K., Gerosa, L., and Sauer, U. (2018) Reserve flux capacity in the pentose phosphate pathway enables *Escherichia coli*'s rapid response to oxidative stress. *Cell Syst. 6*, 569−578.
(38) Brockman, I. M., and Prather, K. L. (2015) Dynamic knockdown of *E. coli* central metabolism for redirecting fluxes of primary metabolites. *Metab. Eng. 28*, 104−113.
(39) Condon, C., Squires, C., and Squires, C. L. (1995) Control of rRNA transcription in *Escherichia coli*. *Microbiol. Rev. 59*, 623−645.
(40) Nodwell, J. R., and Greenblatt, J. (1993) Recognition of boxA antiterminator RNA by the *E. coli* antitermination factors NusB and ribosomal protein S10. *Cell 72*, 261−268.
(41) Berg, K. L., Squires, C., and Squires, C. L. (1989) Ribosomal RNA operon antitermination: Function of leader and spacer region boxB-boxA sequences and their conservation in diverse micro-organisms. *J. Mol. Biol. 209*, 345−358.
(42) Greive, S. J., Lins, A. F., and von Hippel, P. H. (2005) Assembly of an RNA-protein complex. Binding of NusB and NusE (S10) proteins to boxA RNA nucleates the formation of the antitermination complex involved in controlling rRNA transcription in *Escherichia coli*. *J. Biol. Chem. 280*, 36397−36408.
(43) Chatterjee, A., Johnson, C. M., Shu, C.-C., Kaznessis, Y. N., Ramkrishna, D., Dunny, G. M., and Hu, W.-S. (2011) Convergent transcription confers a bistable switch in *Enterococcus faecalis* conjugation. *Proc. Natl. Acad. Sci. U. S. A. 108*, 9721−9726.
(44) Ma, N., and McAllister, W. T. (2009) In a head-on collision, two RNA polymerases approaching one another on the same DNA may pass by one another. *J. Mol. Biol. 391*, 808−812.
(45) Crampton, N., Bonass, W. A., Kirkham, J., Rivetti, C., and Thomson, N. H. (2006) Collision events between RNA polymerases in convergent transcription studied by atomic force microscopy. *Nucleic Acids Res. 34*, 5416−5425.
(46) Hobson, D. J., Wei, W., Steinmetz, L. M., and Svejstrup, J. Q. (2012) RNA polymerase II collision interrupts convergent transcription. *Mol. Cell 48*, 365−374.
(47) Blattner, F. R., Plunkett, G., Bloch, C. A., Perna, N. T., Burland, V., Riley, M., Collado-Vides, J., Glasner, J. D., Rode, C. K., and Mayhew, G. F. (1997) The complete genome sequence of *Escherichia coli* K-12. *Science 277*, 1453−1462.
(48) Kröger, M., and Hobom, G. (1982) A chain of interlinked genes in the ninR region of bacteriophage lambda. *Gene 20*, 25−38.
(49) Mashko, S. V., Veiko, V. P., Lapidus, A. L., Lebedeva, M. I., Mochulsky, A. V., Shechter, I. I., Trukhan, M. E., Ratmanova, K. I., Rebentish, B. A., Kaluzhsky, V. E., and Debabov, V. G. (1990) TGATG vector: a new expression system for cloned foreign genes in *Escherichia coli* cells. *Gene 88*, 121−126.
(50) Gulevich, A. Iu., Skorokhodova, A. Iu., Ermishev, V. Iu., Krylov, A. A., Minaeva, N. I., Polonskaia, Z. M., Zimenkov, D. V., Biriukova, I. V., and Mashko, S. V. (2009) New method of construction of artificial translational-coupled operons in bacterial chromosome. *Mol. Biol. (Moscow, Russ. Fed., Engl. Ed.) 43*, 547−557.
(51) Sambrook, J., and Russell, D. W. (2001) *Molecular cloning: a laboratory manual* 3rd ed., Cold Spring Harbor Laboratory Press, New York.
(52) Datsenko, K. A., and Wanner, B. L. (2000) One-step inactivation of chromosomal genes in *Escherichia coli* K-12 using PCR products. *Proc. Natl. Acad. Sci. U. S. A. 97*, 6640−6645.
(53) Doroshenko, V., Airich, L., Vitushkina, M., Kolokolova, A., Livshits, V., and Mashko, S. (2007) YddG from *Escherichia coli* promotes export of aromatic amino acids. *FEMS Microbiol. Lett. 275*, 312−318.
(54) Airich, L. G., Tsyrenzhapova, I. S., Vorontsova, O. V., Feofanov, A. V., Doroshenko, V. G., and Mashko, S. V. (2011) Membrane topology analysis of the *Escherichia coli* aromatic amino acid efflux protein YddG. *J. Mol. Microbiol. Biotechnol. 19*, 189−197.
(55) Minaeva, N. I., Gak, E. R., Zimenkov, D. V., Skorokhodova, A. Y., Biryukova, I. V., and Mashko, S. V. (2008) Dual-In/Out strategy for genes integration into bacterial chromosome: a novel approach to step-by-step construction of plasmid-less marker-less recombinant *E. coli* strains with predesigned genome structure. *BMC Biotechnol. 8*, 63.
(56) Linn, T., and St Pierre, R. (1990) Improved vector system for constructing transcriptional fusions that ensures independent translation of *lacZ*. *J. Bacteriol. 172*, 1077−1084.
(57) Leveau, J. H., and Lindow, S. E. (2001) Predictive and interpretive simulation of green fluorescent protein expression in reporter bacteria. *J. Bacteriol. 183*, 6752−6762.
(58) Proshkin, S., Rahmouni, A. R., Mironov, A., and Nudler, E. (2010) Cooperation Between Translating Ribosomes and RNA Polymerase in Transcription Elongation. *Science 328*, 504−508.
(59) Knaus, R., and Bujard, H. (1990) Principles governing the activity of *E. coli* promoters in *Nucleic Acids and Molecular Biology* (Eckstein, F., and Lilley, D. M. J., Eds.) pp 110−122, Springer-Verlag, Heidelberg.

https://dx.doi.org/10.1021/acssynbio.9b00463
ACS Synth. Biol. 2020, 9, 1650−1664

(60) Salas, M., Vinuela, E., and Sols, A. (1965) Spontaneous and enzymatically catalyzed anomerization of glucose 6-phosphate and anomeric specificity of related enzymes. *J. Biol. Chem. 240*, 561−568.
(61) Srere, P. (1969) Citrate synthase:[EC 4.1. 3.7. Citrate oxaloacetate-lyase (CoA-acetylating)] in *Citric Acid Cycle. Methods in Enzymology* (Lowenstein, J., Ed.) pp 3−11, Academic Press, New York.
(62) Cánovas, J., and Kornberg, H. (1969) Phosphoenolpyruvate carboxylase from *Escherichia coli* in *Citric Acid Cycle. Methods in Enzymology* (Lowenstein, J., Ed.) pp 288−292, Academic Press, New York.

https://dx.doi.org/10.1021/acssynbio.9b00463
ACS Synth. Biol. 2020, 9, 1650−1664